Available online at www.sciencedirect.com

jmr&t Journal of Materials Research and Technology

journal homepage: www.elsevier.com/locate/jmrt

The influence of intergranular oxidation on surface crack formation in continuous casting of steel

Georg Gaiser [a,*], Roman Krobath [b], Peter Presoly [a], Christian Bernhard [a]

[a] Ferrous Metallurgy, Montanuniversitaet Leoben, Franz-Josef-Strasse 18, 8700 Leoben, Austria
[b] Voestalpine Wire Rod Austria GmbH, Drahtstraße 1, 8792 St. Peter-Freienstein, Austria

ARTICLE INFO

Article history:
Received 20 July 2023
Accepted 20 September 2023
Available online 23 September 2023

Keywords:
Continuous casting
Intergranular oxidation
Silicon
Surface crack formation
IMC-B test

ABSTRACT

High-temperature oxidation phenomena play an important role in steel processing. What is mostly underrated is the importance of internal oxidation in casting processes, namely the continuous casting process. To investigate the impact of intergranular oxidation on surface defect formation, experiments for two cooling strategies and time sequences for a conventional slab caster were conducted. As the influence of silicon on high-temperature oxidation is well known and its effect on surface ductility is marginal silicon was chosen as an alloying element to provoke intergranular oxidation. The methods used were the In-Situ Material Characterization by Bending test (IMC-B), which provides the investigation of the susceptibility to surface crack formation by 3-point bending under oxidizing testing conditions and simultaneous thermal analysis for the well-controlled study of high-temperature oxidation phenomena. The results show that during a cooling cycle supporting highly oxidizing conditions, silicon favors the formation of a low-melting eutectic ($FeO-Fe_2SiO_4$) at the interface, infiltrating the steel along the austenite grain boundaries. The intergranular oxidation formed has a depth of less than 50 μm but leads to a stress concentration during a subsequent tensile deformation. In consequence, cracks may easily nucleate and propagate along austenite grain boundaries. A change in the steel composition by reducing the silicon content to almost zero or a less harmful temperature sequence reduces intergranular oxidation and subsequently the susceptibility to crack formation.

1. Introduction

Steelmaking processes have improved concerning productivity and product quality over decades. This applies particularly to continuous casting, where in parallel, process automation and quality control systems are steadily enhanced. Besides internal quality, attention is mainly paid to surface quality. For state-of-the-art continuous casting machines with highly advanced operating systems, reliable control of most macroscopic defects is possible.

The classical phenomena behind the influence of phase transformations and grain sliding on high-temperature ductility are generally well understood [1]. Nevertheless, microscopic defects may also form along grain boundaries under the oxide scale layer [2]. They can occur network-like and transversally with a typical depth of less than 1 mm. This phenomenon may also be related to the formation of coarse austenite grains due to the appearance of local depressions or deep oscillation marks on the surface, sometimes referred to as “crazing” or “blown grains” [3].

* Corresponding author
E-mail address: georg.gaiser@unileoben.ac.at (G. Gaiser).
https://doi.org/10.1016/j.jmrt.2023.09.214

Among the already mentioned influences, selective oxidation processes are considered a reason for such defects [4]. High temperature accelerates the oxidation processes. When the strand leaves the mold, unavoidable oxidation processes occur. The risk of defect formation is even higher when certain hot spots on the strand surface appear, e.g. in the course of surface depressions already forming in the mold, like deep oscillation marks or off-corner depressions.

External and internal oxidation can generally be divided: External oxidation processes lead to scale growth on the strand surface and cause yield loss. The high availability of oxidizing atmosphere propagates external oxidation. In contrast, lower availability of oxygen favors internal oxidation processes, particularly intergranular oxidation, causing preliminary damage in the surface and sub-surface area of the austenite grain boundary and finally affecting the crack nucleation during secondary cooling and in the subsequent straightening process [4].

A further consequence of grain boundary oxidation may be the appearance of liquid metal embrittlement in steels containing low melting tramp elements like copper, tin and antimony. During oxidation, these elements enrich at the steel/scale interface due to their low affinity to oxygen. If the solubility is exceeded, a metallic copper phase is formed, which is liquid or solid, depending on the oxidation temperature. A liquid metal phase is able to penetrate the steel, particularly along the austenite grain boundaries, and causes liquid metal embrittlement or surface hot shortness, respectively [5–17].

Additionally, silicon alloyed steels form a liquid phase on the steel surface at a sufficient oxidation temperature. Silicon oxidizes to SiO_2 and forms with FeO, a low-melting eutectic ($FeO–Fe_2SiO_4$; T_s ~1185 °C) [18]. Oxidation processes at temperatures exceeding the eutectic temperature cause a substantial accumulation of the low melting eutectic in the interface area. The liquid phase penetrates the grain boundaries of the base material and the scale [19–25]. Due to increased scale adhesion, this phenomenon has been the subject of various investigations, especially dealing with the problem of rolling defects [21,26,27]. The depth of intergranular oxidation produced by the liquid phase depends on the Si content and oxidation time. Even for short oxidation times, intergranular oxidation can reach a depth of around 20 μm [24].

An additional source of intergranular oxidation is the formation of an oxide layer in the close range of grain boundaries. The oxide layer consists of elements with a high affinity to oxygen, like Al, Si, Mn and Ti [28–32].

All previously stated oxidation phenomena may also appear in the continuous casting process, where the hot strand surface is commonly cooled by an air/water mixture, resulting in a high oxidation potential. The subsequent appearance of intergranular oxidation should result in an increasing crack susceptibility. As outlined before, Si is an alloying addition in most steels and has a decisive influence on high-temperature oxidation. The direct impact on hot ductility and crack susceptibility of steel in casting machines is marginal. Therefore, the focus of this work is to provoke intergranular oxidation formation by adding Si for different cooling cycles and investigate the effect on surface defect formation in a subsequent bending test. The tests were performed with the In-Situ Material Characterization by Bending test (IMC-B), simulating oxidation and surface defect formation of directly cast samples under continuous casting conditions. In addition, oxidation tests carried out by simultaneous thermal analysis (STA) were applied in parallel to simulate the oxidation in the IMC-B test under controlled conditions to investigate whether the time and cost-saving but well-controllable STA experiments can allow indicating crack susceptibility of steel under the given cooling and oxidation conditions.

2. Experimental section

The chemical composition of the steel grades for the test series presented is shown in Table 1. Except for Si, the chemical composition remains constant for all elements. The given chemical analysis of the individual elements refers to the mean value of all samples examined in this study. Steel 2 represents the standard composition of the investigated construction steel.

2.1. *IMC-B test*

The IMC-B test was developed at Montanuniversitaet Leoben, representing a testing method for characterizing the material behavior of cast steel samples after controlled cooling in oxidizing at elevated temperatures. The aim of the method is the experimental simulation of the susceptibility to surface defect formation for continuous casting processes. A detailed description is given in former publications [4,33]. The process and main advantages can be briefly summarized as follows:

- Every sample is prepared for casting in an induction furnace. To simulate fast solidification in the mold and cooling, as indicated by the dotted lines in Fig. 1, the sample is cast in the IMC-B mold. Both, the solidification structure, and the final microstructure of the sample after air cooling correspond to that of the strand shell [33–35].

- Mechanical deformation of the sample is attained by an isothermal three-point bending procedure under conditions as close as possible to the straightening of the strand in continuous

Table 1 – Chemical composition of the three investigated steel-grades.

Steel	Chemical composition [wt.%]								
	C	Mn	Si	P	S	Σ (Cu, Ni, Sn)	Al	N	Fe
Steel 1			<0.05						
Steel 2	0.16	1.52	0.37 to 0.42	0.01	0.003	<0.050	0.035	<0.008	bal.
Steel 3			0.68 to 0.85						

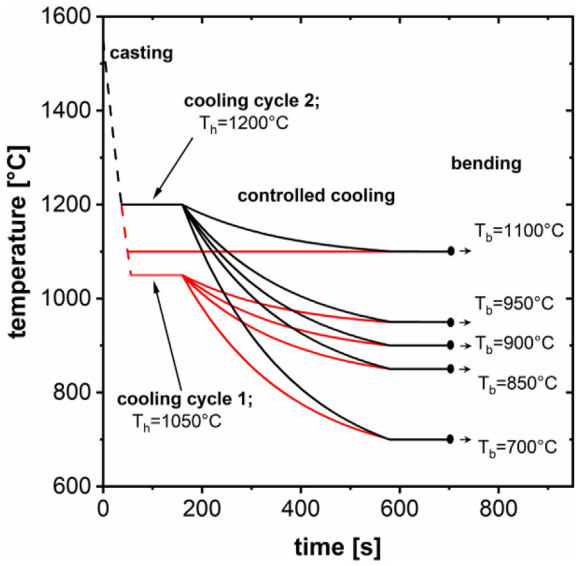

Fig. 1 – Investigated cooling cycles.

casting. The stamp velocity and displacement are the same for all experiments. The maximum tensile strain values on the sample surface amount to 6.3% with maximum strain rates 4.7 $10^{-4}\,s^{-1}$ [33]. These strain rates are in the range of straightening operations in continuous casting [36]. An elasto-viscoplastic material 3D-FE model, parameterized in Abaqus, is used to calculate the stress and strain state during testing [37].

The thermal cycles applied in this work are shown in Fig. 1. Cooling cycle 1 simulates a mold exit temperature of ~1180 °C, subsequent holding at 1050 °C and finally, slow cooling to the bending temperature. Cooling cycle 2 represents the thermal history of a surface depression or a deep oscillation mark. The sample temperature after removal from the mold is approximately 1280 °C, and homogenization follows at 1200 °C. After homogenization at 1050 or 1200 °C, the samples are cooled to the bending temperatures 700, 850, 900, 950 and 1100 °C. The time between the start of casting and the start of homogenization in the bending furnace before bending is adjusted to 580 s. An exception is the bending test at 1100 °C for cooling cycle 1, where the sample is directly cooled to the bending temperature after removal from the mold, but like before, the time until homogenization is adjusted to 580 s. After homogenization, bending starts at 700 s for a total of 175 s (125 s loading, 50 s unloading). The complete experiment is finished after 875 s. This represents the typical casting time until straightening in a slab caster with 1.2 m min^{-1} casting speed [38]. The significant parameters of the testing sequences are listed in Table 2.

Previous results under the same testing conditions indicated a high crack susceptibility of steel 2 at a bending temperature of 900 °C, whereas bending temperatures of 700 °C and 1100 °C resulted in only a few cracks [4]. After descaling with citric acid, the bent samples are investigated for surface defects in the strain-influenced area with a digital microscope Keyence VHX7000; see Fig. 2, with the cracks indicated in red. The crack detection procedure provides the total number of intergranular cracks and the critical strain for first crack formation ε_2 on the sample surface [33].

2.1.1. *Oxidation investigations on IMC-B samples*

The samples from the IMC-B test are investigated for intergranular oxidation as a result of thermal history and steel. Samples of steel 3 and thermal cycle 2 with bending temperatures of 1100, 900 and 700 °C - see Fig. 1 - were investigated in order to show differences in the oxidation state. In addition, the samples of all steels with a bending temperature of 900 °C were compared and for steel 2, the sample for cycle 1 was also examined. The significant points for temperature sequences are listed in Table 2.

The examination took place in a strain-free zone, which means that any influence by the bending test can be excluded; see Fig. 2. For the best possible protection of the casting condition, the whole area besides the support left of the examined bending specimen was directly cold-embedded without any processing, which ensures optimal protection of the interface steel/scale in the subsequent cutting operations and a more straightforward handling during grinding and polishing (diamond suspension, 9 μm and 3 μm). For particular measurements, the finished samples were etched with nital solution (3% HNO_3) or picric solution. Cross-sections were observed by optical microscopy (Polyvar Reichert-Jung MEF 2 and Keyence VHX7000) and scanning electron microscopy (SEM, JEOL FE-SEM 7200F). Investigations with SEM require an appropriate conductivity of the sample, which was ensured by sputtering the entire sample surface with a thin carbon layer (~10 nm). In every metallographic examination, the intergranular oxidation depth was measured and the number of intergranular oxidations was determined. The appearing phases were analyzed by SEM/EDS.

2.2. *STA oxidation experiments*

For reproducing the intergranular oxidation from the IMC-B samples, oxidation experiments on a simultaneous thermal analysis (Netzsch STA 449 F3 Jupiter with a SiC furnace and a DTA-TG sample carrier) were carried out. The gas inlet is located on the bottom of the furnace (inner diameter 26.5 mm) and the gas outlet is situated on the top side of the furnace. The dimensions of the oxidation samples are 13 × 12.2 × 2 mm. The material for this investigation was cut from the samples already used for the oxidation investigations of the IMC-B samples to guarantee identical chemical composition. The cutting was performed with a wet abrasive cutting machine - ATM Brilliant 220. A hole of 2.5 mm in diameter was drilled to

Table 2 – Important marks in the testing sequence.

Cooling cycle	Mold cooling [s]	T after mold [°C]	T holding step [°C]	t after holding [s]	t bending start - end [s]	T in-situ bending test [°C]	T oxidation investigation [°C]
1	45	~1180	1050	160	700–875	700, 850, 900, 950, 1100	900
2	35	~1280	1200				1100, 900, 700

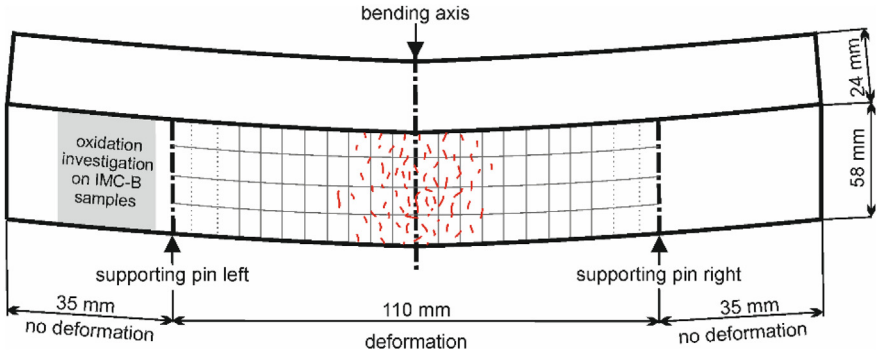

Fig. 2 – Scheme of the IMC-B sample.

secure the suspended specimen. To avoid contamination of the sample, a cleaning step with ethanol and acetone was performed immediately before any experiment. One of the main objectives of the STA oxidation experiment, besides reproducing the results from the IMC-B tests, is to predict the intergranular oxidation in future IMC-B tests and thus estimate how oxidation will affect cracking.

All samples were heated to 1320 °C and held at this temperature for 10 min. The homogenization step ensures the uniform condition of the samples and leads to the necessary grain growth to compensate the grain size reducing phase transformation which occurs during heating. The heating and the isothermal holding steps were performed in an argon 5.0 atm. Depending on the steel and underlying cooling cycle to be investigated, the samples were slowly cooled to the respective shaping temperature of the IMC-B test, followed by another homogenization step for 1 min. Afterward, the atmosphere was switched from argon to synthetic air (20 vol% O_2 and 80 vol% N_2) and the samples were cooled according to the measured temperature profile from the IMC-B test for a total of ~840 s. As a final step, the samples were cooled to room temperature. The amount of oxidation gas was set to 249 ml min^{-1}, which refers to the calibration temperature of the mass flow controller. This corresponds to a gas velocity in the furnace in the range of 3.1–5.0 cm s^{-1}, depending on the respective oxidation temperature. According to a previous publication, laminar flow conditions in the furnace can be assumed for all experiments [39]. Fig. 3 shows a schematic reconstructed cooling cycle for a bending temperature of 900 °C. The first vertical line represents the switch point from argon to synthetic air and marks the first contact with air after the mold in the IMC-B cooling cycle; see Table 2 "mold cooling time". The metallographic preparation and examination of the STA samples were similar to the oxidation investigations of IMC-B samples and described in more detail in a former publication [39].

3. Results

3.1. *Intergranular oxidation*

In Fig. 4 (a), the cross-section of a nital-etched oxidation sample is shown. The red dashed lines indicate former austenite grain boundaries. At the steel/scale interface, the formation of intergranular oxidation is clearly visible. The detail shows exemplarily the depth measurement of intergranular oxidation on an unetched sample; see Fig. 4 (b) To exclude changes at the interface due to etching, all the oxidation samples were evaluated in an unetched condition. A minimum depth of 10 μm was set as the evaluation limit for the measurement of intergranular oxidation to avoid confusion with other surface artefacts. In order to ensure a representative evaluation of the measured intergranular oxidation, a minimum number of at least 10 defects was defined for the evaluation.

Fig. 5 (a) shows the average intergranular oxidation depth and the frequency of occurrence for all three steels and bending temperatures of 900 °C. The IMC-B oxidation investigations are displayed as empty bars and the STA oxidation tests are exhibited in a dark shade. In addition, a comparison between the two cooling cycles examined is presented for the IMC-B oxidation investigation of steel 2 as a hatched bar. By examining the contrast between cooling cycles 1 and 2, the higher temperature after the mold and holding temperature for cooling cycle 2 drastically influence the formation of intergranular oxidation. For steel 2 and

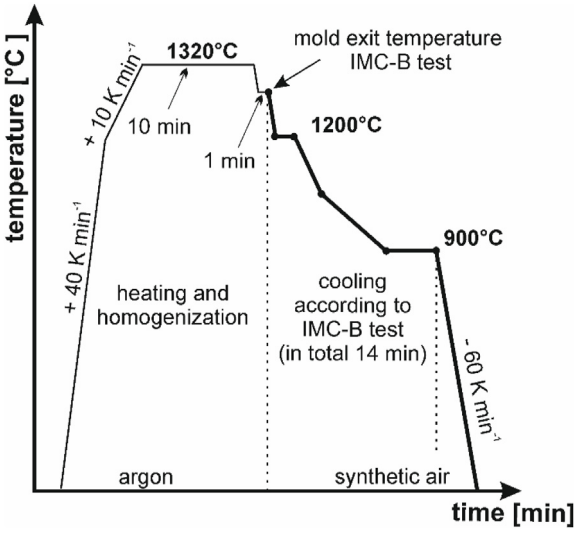

Fig. 3 – Schematic illustration of the investigated STA time-temperature-atmosphere program.

Table 3 – Summary of all oxidation experiments performed.

Steel	Test	Cooling cycle; bending temperature	Average value [μm]	Standard deviation [μm]	Number []
Steel 1	IMC-B	2; T_b = 900 °C	/	/	/
	STA	2; T_b = 900 °C	13.1	3.2	12
Steel 2	IMC-B[a]	1; T_b = 900 °C[a]	13.3[a]	4.2[a]	2[a]
	IMC-B	2; T_b = 900 °C	16.3	5.3	94
	STA	2; T_b = 900 °C	20.7	5.7	118
	STA	2; T_b = 900 °C	21.3	6.1	123
Steel 3	IMC-B	2; T_b = 700 °C	19.9	7.6	109
	STA	2; T_b = 700 °C	19.7	5.5	105
	STA	2; T_b = 700 °C	21.0	5.8	101
	IMC-B	2; T_b = 900 °C	19.2	5.9	95
	STA	2; T_b = 900 °C	19.3	5.2	93
	IMC-B	2; T_b = 1100 °C	16.1	4.1	17
	STA	2; T_b = 1100 °C	18.1	6.1	61

/ … no data.
[a] … insufficient, not representative data.

cooling cycle 1, there is hardly any intergranular oxidation present. In total, only two defects are documented. Therefore, the values are not representative and not considered in Fig. 5 (a). In contrast, cooling cycle 2 has an average intergranular oxidation depth of 16.3 μm, with a significantly higher total number. For cooling cycle 2, the silicon-free steel 1 shows no intergranular oxidation. A rise in Si content increases intergranular oxidation depth to 16.3 μm for steel 2. Steel 3 shows the highest intergranular oxidation depth with 19.2 μm. The total number of intergranular oxidations is equal for steels 2 and 3, with almost 95. The mean depth of intergranular oxidation for steel 1 of the STA oxidation experiment is around 13.1 μm, with a total number of 12 defects observed, which contrasts with the absence of intergranular oxidation for the IMC-B oxidation investigation. Nevertheless, both mean depth and total number of defects is relatively small compared to steels 2 and 3. The intergranular oxidation depth for steels 2 and 3 is about 19–21 μm. For steel 3, this result corresponds to that of the IMC-B oxidation investigation, whereas for steel 2, a significant increase in the mean depth occurred.

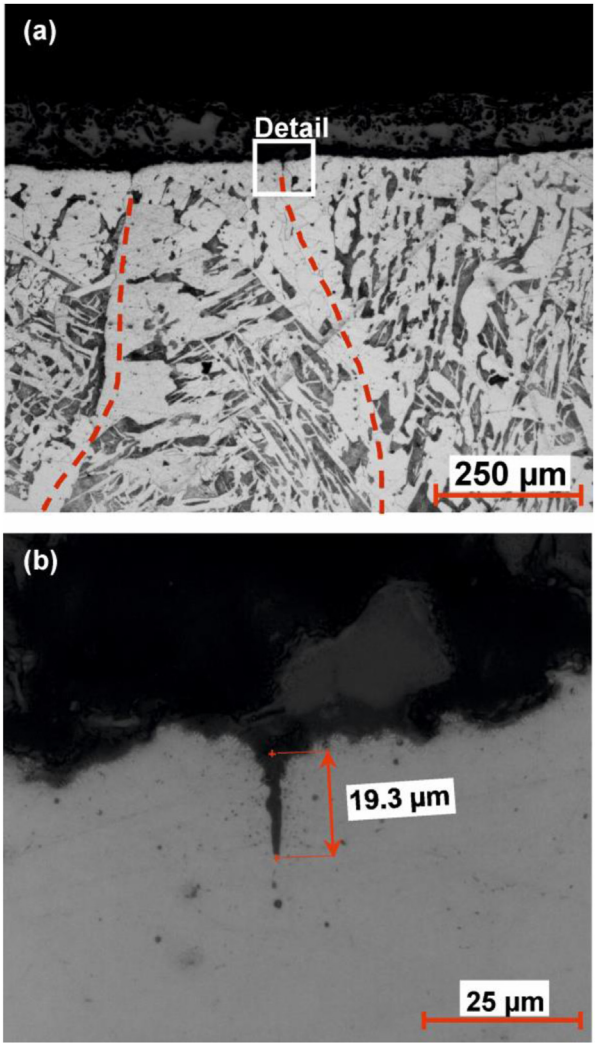

Fig. 4 – (a) Cross-section of an oxidation sample (nital-etched); (b) Detail of the interface with a measured intergranular oxidation depth (unetched).

The influence of the bending temperature on the formation of intergranular oxidation was also investigated. For steel 3 and cooling cycle 2, an increasing bending temperature decreases intergranular oxidation noticeably. Bending at a temperature of 700 °C shows the highest observed intergranular oxidation depth with 19.9 μm and a bending temperature of 1100 °C the lowest, with 16.1 μm. The bending temperature of 900 °C with 19.2 μm is in between. The results are displayed in Fig. 5 (b) as empty bars for the IMC-B oxidation investigation and with dark shading for the STA oxidation test. Both oxidation tests confirm the trend where intergranular oxidation decreases slightly with an increase in bending temperature. The STA oxidation experiment of steel 2 and steel 3 at a bending temperature of 700 °C was performed twice to ensure reproducibility. The mean values of the intergranular oxidation depths differ only slightly from the first experiment, and the total number of intergranular oxidations observed is nearly the same. All results of the oxidation tests are summarized in Table 3. Except for steel 1 and the experiment for cooling cycle 1, the standard deviation hardly shows any differences. The qualitative mapping shown in Fig. 6 reveals strong Si and O enrichment at the former austenite grain boundary and the resulting

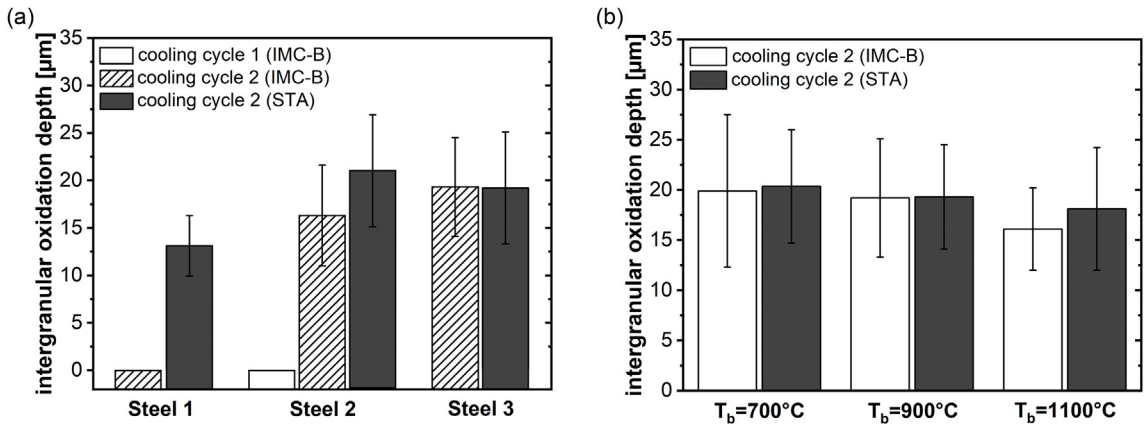

Fig. 5 – (a) Intergranular oxidation depth of the investigated steels and cooling cycles for a bending temperature of 900 °C; (b) Dependence of the intergranular oxidation on the bending temperature for steel 3.

intergranular oxidation. Fig. 7 (a) shows a quantitative spectrum analysis for steel 2. The measured composition is similar to the low-melting eutectic and confirms its presence. The observed $FeO–Fe_2SiO_4$ distribution is identical to the one described by Zhou et al. [40]. The oxide layer around the intergranular oxidation and along the interface consists predominantly of manganese and silicon oxides; see Fig. 7 (b).

3.2. *Surface cracks*

Without going into detail, the reduction in ductility in a certain temperature range basically depends on the formation of precipitates (e.g., aluminum nitride) and the formation of new phases or phase transformations [41,42]. Silicon, frequently used as an alloying element, has not shown any significant negative influence on the surface ductility so far.

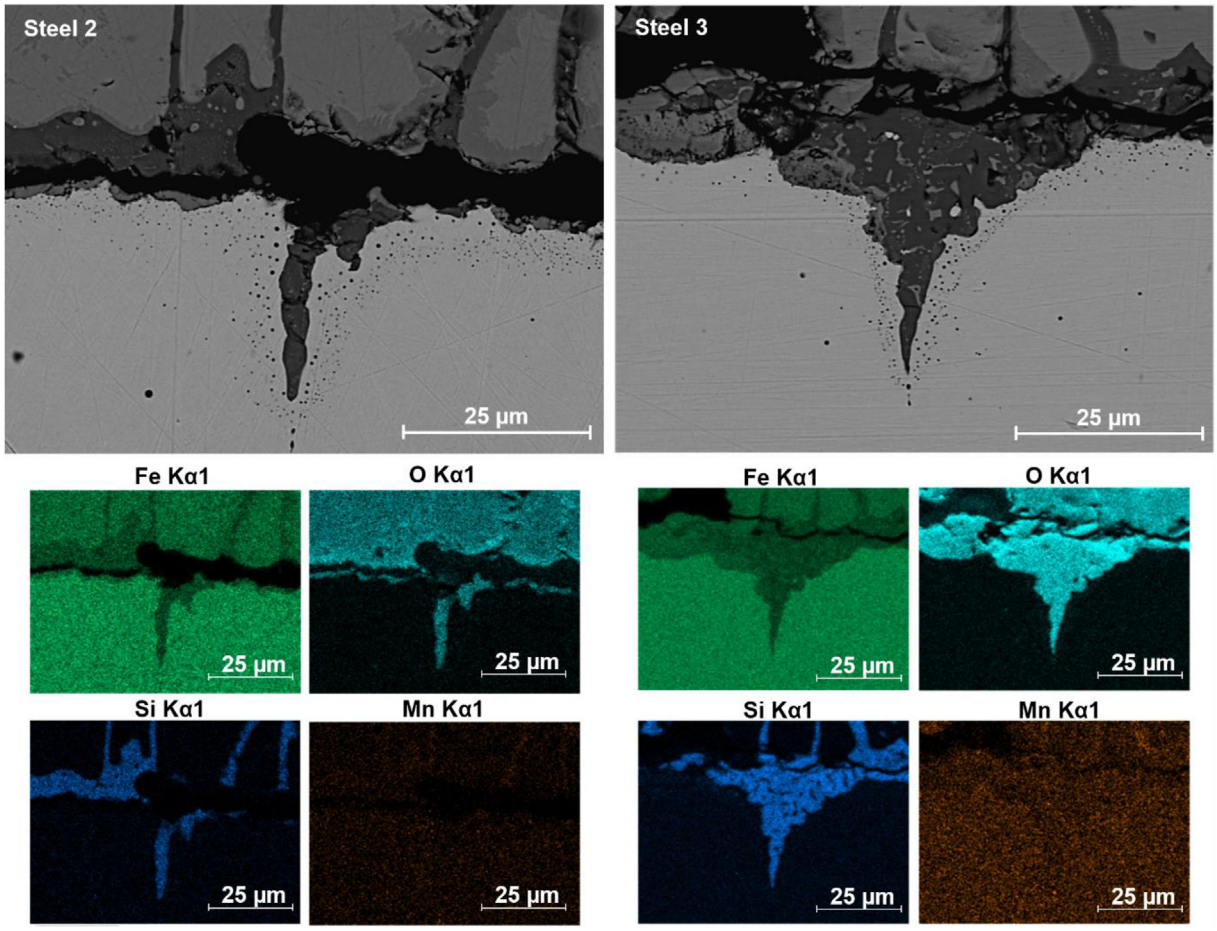

Fig. 6 – SEM image from the interface with qualitative element distribution for steels 2 and 3 (cooling cycle 2; $T_b = 900$ °C).

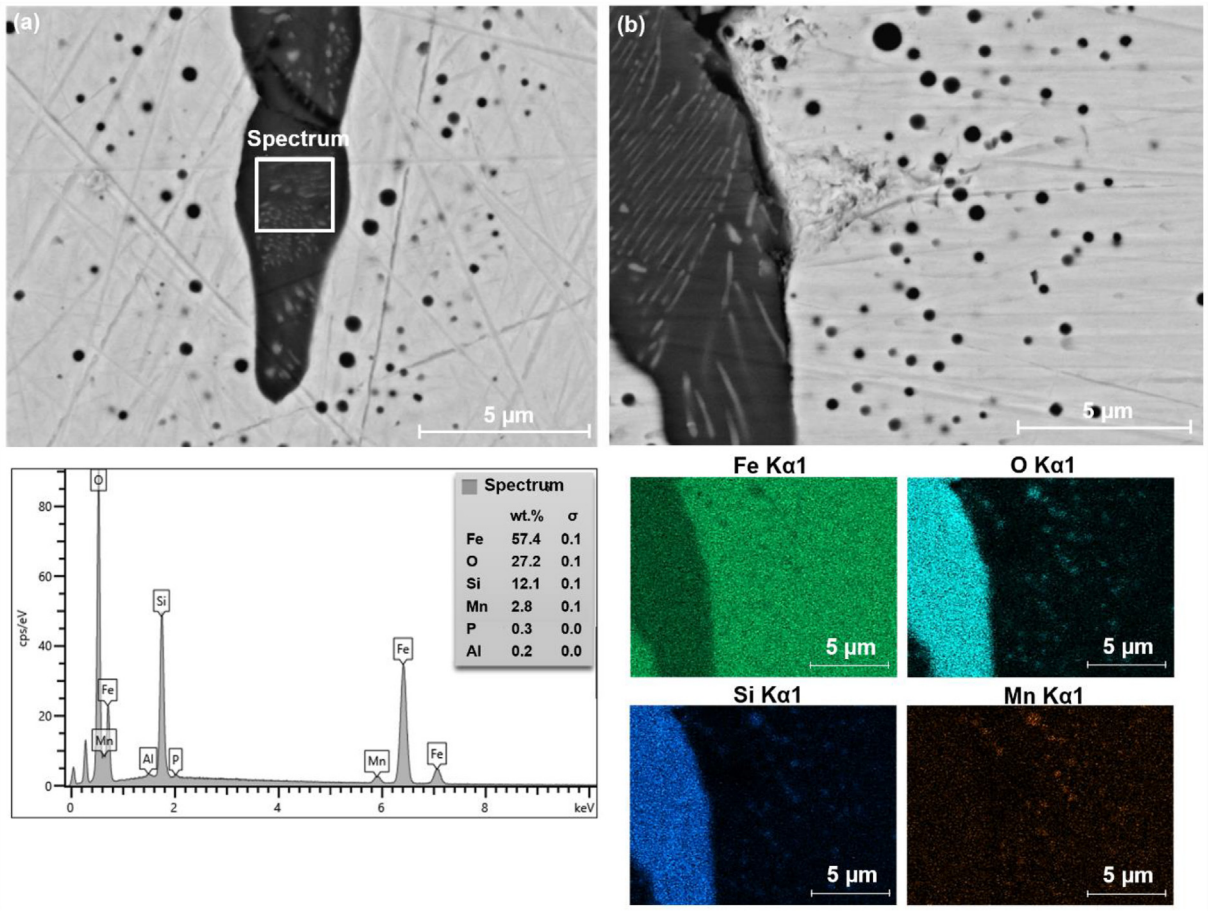

Fig. 7 – (a) Quantitative spectrum analysis of the intergranular oxidation for steel 2; (b) Detail of the internal oxide layer.

However, silicon and its tendency to form liquid phases at sufficiently high oxidation temperatures can lead to intergranular oxidation phenomena, which further intensify already existing ductility-reducing effects. For steel 2, a detailed investigation of the ductility reducing mechanisms was performed by Krobath et al. [4] which will not be further discussed in this publication. However, it is also valid for steel 1 and 3 as silicon hardly influences surface ductility. The focus in this publication is on the influence of intergranular oxidation on surface crack formation in continuous casting.

Fig. 8 compares the crack distributions for the samples of cooling cycle 2 in the temperature range of 700, 850 to 950 and 1100 °C. Furthermore, it shows the optical differences in crack distribution for steel 2 between cooling cycle 1 and cooling cycle 2. The surface is divided into segments, where white describes a segment free of cracks, yellow means one to five cracks and a red segment shows more than five cracks. Segments with a grid structure illustrate crack networks that display a very high number of orientated and partially unoriented cracks, which can be directly related to pre-defects like intergranular oxidation. The results of cooling cycle 2 clearly indicate an increase in the documented cracks with rising Si content in the area of the bending axis and in the outer segments of the bending samples. As a result of the intensified oxidation for cooling cycle 2, the cracks around the bending axis appear more network-like and the formation of the first cracks occurs further away from the bending axis.

According to Krobath et al. [4], the maximum number of cracks on the entire sample is set at 800, since a significant differentiation of individual cracks is hardly possible for numbers exceeding this limit. Fig. 9 (a) and (b) show the total number of detected cracks and the critical strain ε_2 for first crack formation. The light red area in Fig. 9 (b) represents strain values which can be considered critical for straightening in continuous casting [3,41]. For cooling cycle 2, all three steels were investigated, while for cooling cycle 1, only steel 2 was examined. The results of steel 2 at 700, 900 and 1100 °C refer to a previous publication by Krobath et al. [4].

At a bending temperature of 700 °C, hardly any surface cracks are formed for all investigated steel grades. A total of eight cracks were documented for steel 3. Steels 1 and 2 are crack-free. For the bending temperatures 850, 900 and 950 °C, the number of documented surface cracks for steel 2 and cooling cycle 1 amount to 228, 177 and 141, respectively. These values are larger than those of steel 1, although it was cooled according to cooling cycle 2. For steel 1, the number of documented surface cracks adds up to 153, 158 and 49. A massive impact of the cooling cycle can be seen by comparing the steel

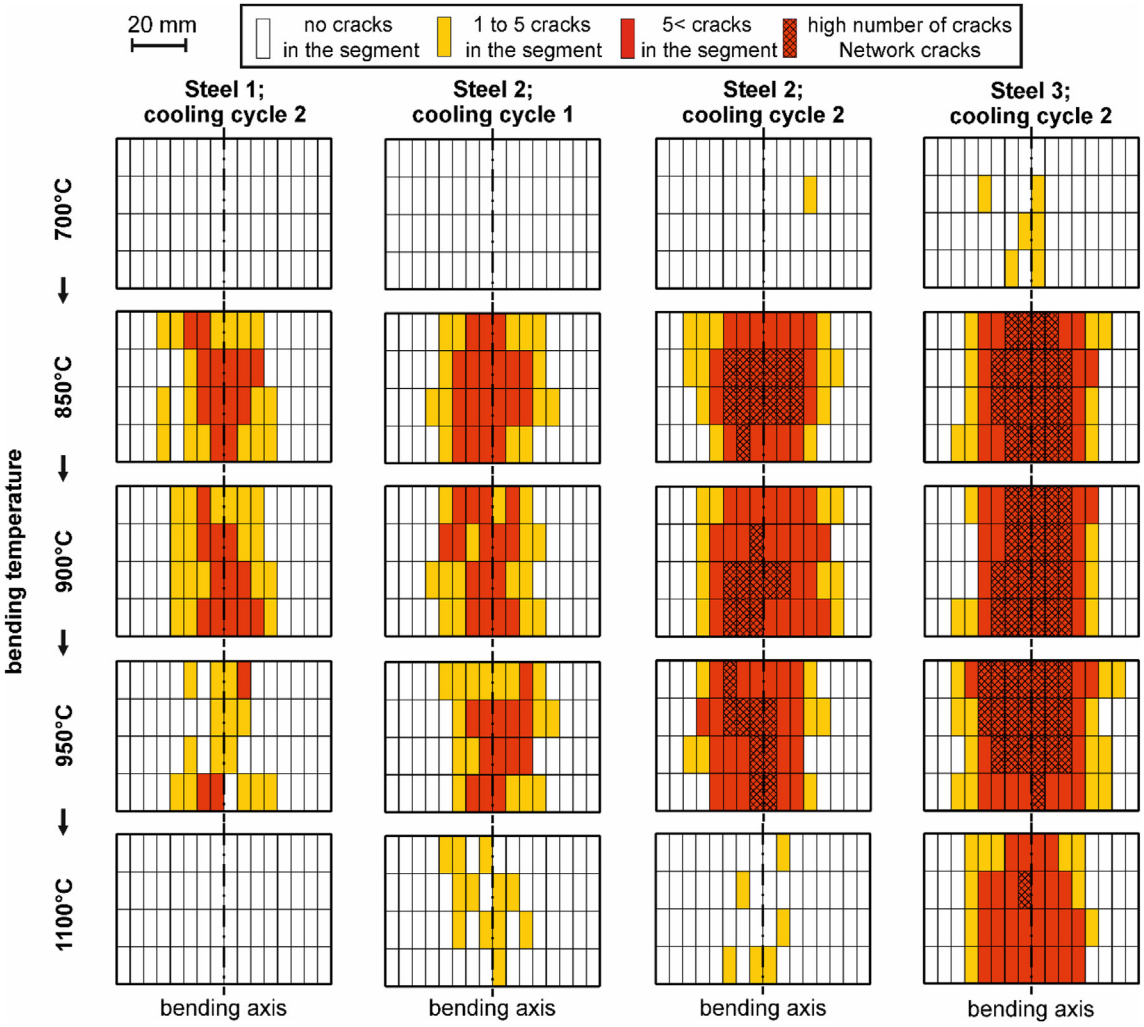

Fig. 8 – Crack distribution for all investigated cooling cycles and samples.

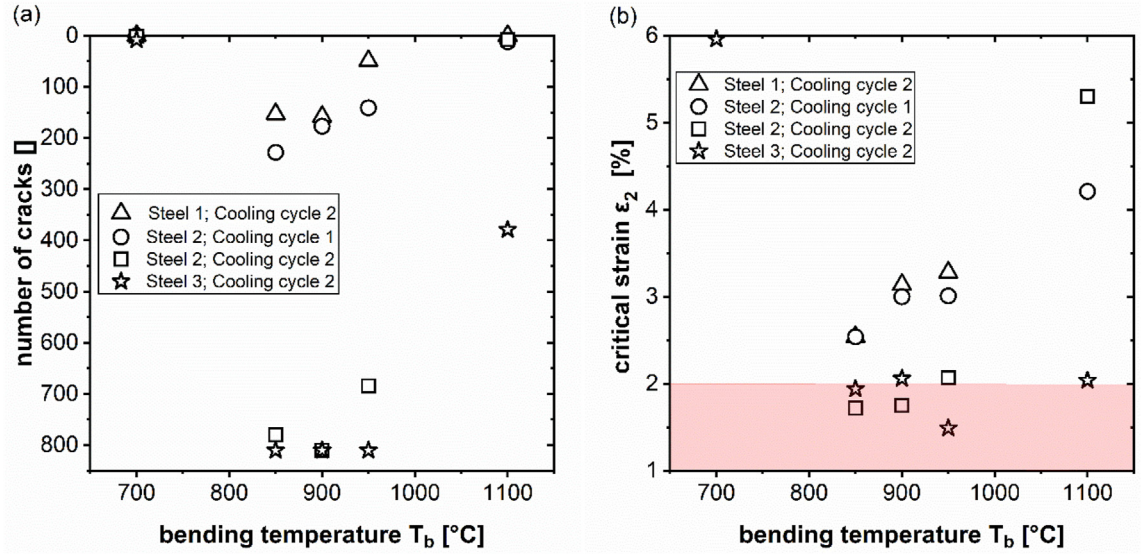

Fig. 9 – Results of the IMC-B test: (a) Total number of cracks; (b) Critical strain ε_2.

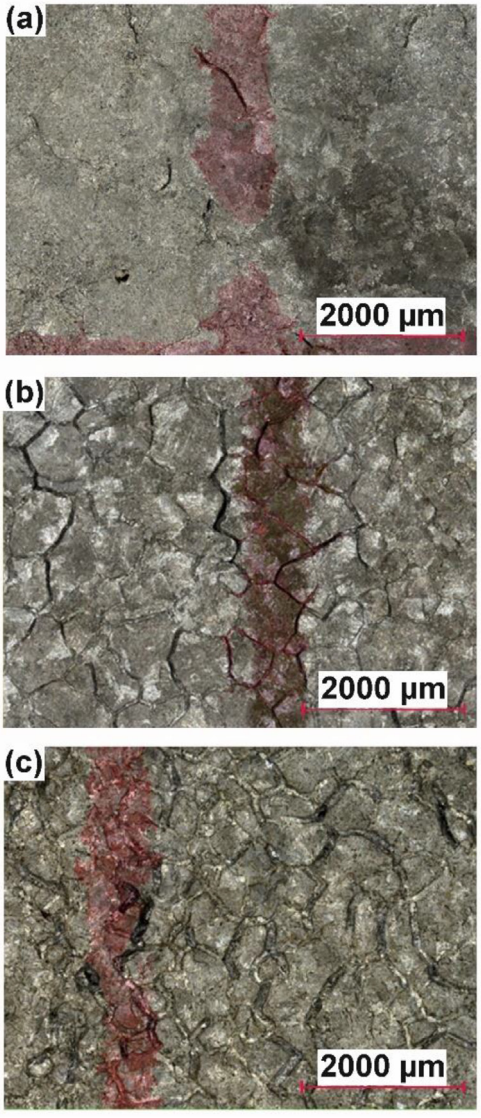

Fig. 10 – Comparison of the surface in the area of the bending axis for cooling cycle 2: (a) steel 1; (b) steel 2; (c) steel 3.

2 results. The number of cracks increases dramatically to 780, 800 and 690, respectively, in the investigated temperature region. For steel 3, more than 800 cracks were documented for all three bending temperatures. Therefore, to compare pronounced crack sensitive testing sequences, only the number of cracks as an evaluation parameter is not sufficient to determine a difference anymore. The critical strain ε_2 is more suitable as an additional evaluation parameter. At 1100 °C, significant differences between the steels can be observed. While steel 1 is without cracks and alloy 2 has about 10 cracks, steel 3 has a total of 379 cracks.

For the critical strain, which by definition requires two or more cracks, only steel 3 falls into this category with a value of 6% at a bending temperature of 700 °C. Regarding the bending temperatures 850–950 °C, the critical strain for steel 1 with cooling cycle 2 and steel 2 with cooling cycle 1 is almost the same, with the lowest value of 2.5% at a bending temperature of 850 °C. For 900 and 950 °C, the values are about 3%. For steels 2 and 3, which were cooled with cooling cycle 2, the values for the critical strain are in the range of 2% or lower. At 850 and 900 °C, the critical strain of steel 2 is approximately 1.7%, and at 950 °C it increases slightly to 2.1%. For steel 3, the critical strain values at 850 and 900 °C are marginally higher in comparison to steel 2, with 1.9 and 2.1%, respectively. The lowest value of steel 3 was documented at 950 °C with 1.5%. At 1100 °C, no critical strain can be determined for steel 1 since no cracks are formed. For steel 2, the critical strain ranges from 4 to 5%. The potential for cracking is highest for steel 3 at around 2.1%.

Depending on the Si content, the crack morphology shows significant differences. While steel 1 only shows singular cracks with a maximum length of a few 100 µm, steel 2 and steel 3 are covered in crack networks. The appearing crack networks are substantially wider and have a crack length of several millimeters. Fig. 10 shows a comparison of the crack pattern in the area of the bending axis (vertical red line). For steels 1 and 2, the picture was taken at bending temperature 850 °C and for steel 3 at 950 °C.

4. Discussion

4.1. *Oxidation*

The SEM analyses have proven that intergranular oxidation forms due to the low-melting eutectic. The differing results concerning intergranular oxidation depth and frequency greatly depend on the underlying cooling cycle and the Si content. The essential aspects of the oxidation investigations will be discussed below:

Regarding cooling cycle 1, the average temperature of 1180 °C after the mold is slightly higher than that of the fayalite eutectic, but due to the rapid cooling afterward, there is hardly any time to form significant amounts of the $FeO–Fe_2SiO_4$ eutectic phase. The formation of intergranular oxidation is low and occurs only sporadically.

For cooling cycle 2, the high temperature after the mold and the homogenization temperature $T_h = 1200$ °C leads to sufficient formation of the liquid eutectic, which favors intergranular oxidation. As a consequence of Si content lower than 0.05 wt%, hardly any liquid fayalite eutectic is formed for steel 1 during the first cooling and homogenization, resulting in almost no intergranular oxidation. In comparison, the intergranular oxidation depth for steels 2 and 3 is significantly higher. With increasing Si content, the amount of the formed liquid eutectic phase rises. In the IMC-B oxidation investigation, the intergranular oxidation depth for steel 3 is increased compared to steel 2. The total number of intergranular oxidations stays approximately the same for steels 2 and 3. This indicates that even for steel 2, the amount of liquid eutectic is sufficient to infiltrate all superficial grain boundaries and generate intergranular oxidation.

Furthermore, it is possible to reproduce the results from the IMC-B tests using simultaneous thermal analysis and the results essentially correspond to those of the IMC-B oxidation investigation. Contrary to the IMC-B sample, the intergranular oxidation depth of steel 2 at a bending temperature of 900 °C is

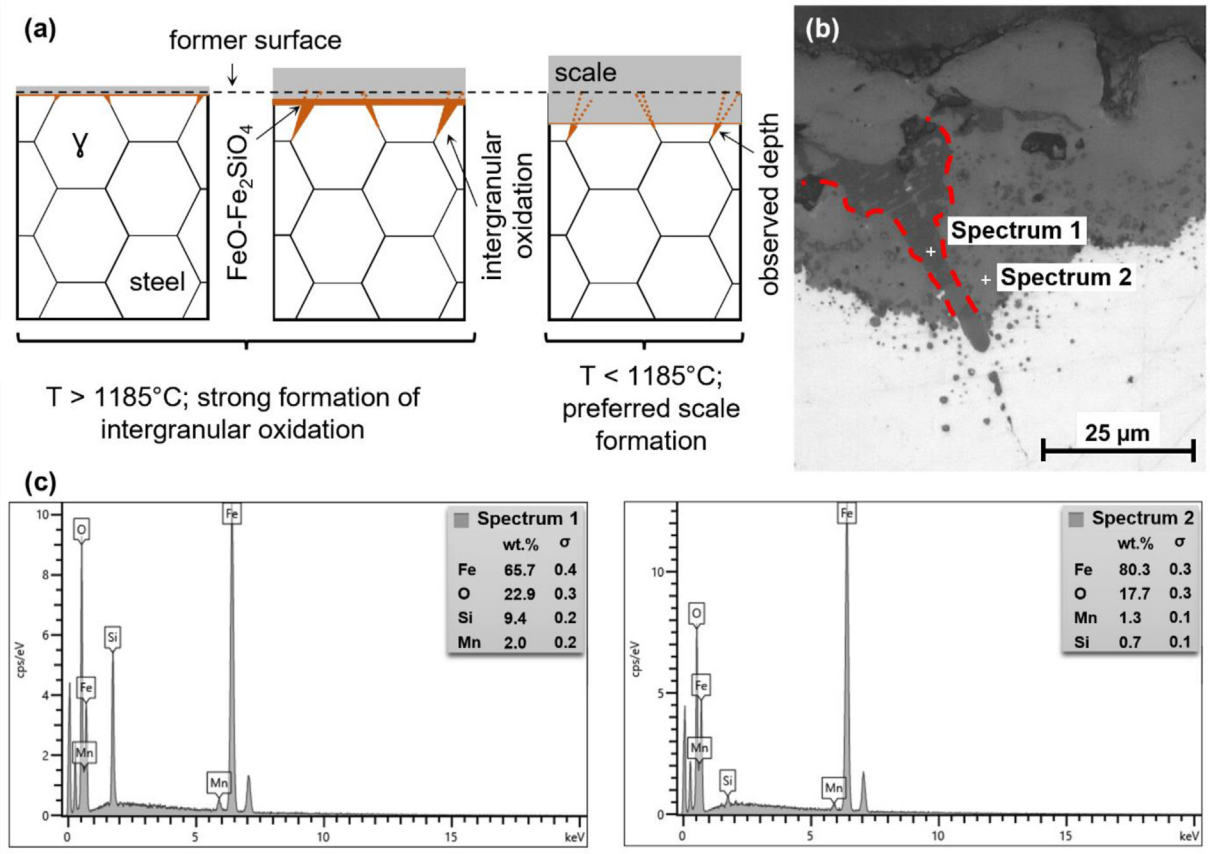

Fig. 11 – (a) Schematic illustration of the temperature dependency on the growth of intergranular oxidation; (b) Reduction of intergranular oxidation depth due to scaling; (c) chemical analysis of the appearing phases.

increased and the value is even slightly higher than that of steel 3. As this test is repeated, it reveals similar results, thus a one-time occurrence can be excluded. This rather unexpected behavior is likely to be multifaceted and, therefore, difficult to fix on a single mechanism, like slight differences in the experimental setup regarding the gas supply, sample size, or a localized scale detachment. The real reason remains unknown. Nevertheless, the experimental setup of the STA has proven to be a fast and useful tool for the investigation of intergranular oxidation, allowing the future prediction of the state during bending in the IMC-B tests.

For both test methods, an influence of the bending temperature on the mean intergranular oxidation depth can be determined for steel 3, whereby an increase in the bending temperature causes a reduction in the intergranular oxidation depth. This is particularly pronounced in the sample with the highest bending temperature of 1100 °C. With increasing bending temperature, the oxidation time in the high-temperature range of the sample rises, so scaling increases. The formation of intergranular oxidation due to a liquid fayalite phase is limited to a temperature range higher than the melting point. In relation to the equilibrium system FeO–SiO_2 [18], this temperature is at least ~1185 °C. Below this temperature, the liquid phase solidifies and cannot penetrate further into the steel. The depth can no longer increase. Further scaling of the sample leads to a continuous decrease in the intergranular oxidation depth. The processes described are illustrated schematically in Fig. 11 (a). Kizu et al. [25] reported a similar mechanism regarding depth progression for isothermal oxidation experiments. Fig. 11 (b) shows the practical appearance of steel 3 at a bending temperature of 1100 °C. The dashed lines represent the original intergranular oxidation depth. Due to subsequent scaling below the eutectic temperature, the depth was significantly reduced. A quantitative analysis is shown in Fig. 11 (c). The chemical analysis of the former intergranular defect indicates similar silicon enrichment as in Fig. 7 (a) and spectrum 2 primarily corresponds to iron oxides. The schematic illustration of the polygonal grain structure in Fig. 11 (a) corresponds to a reheated microstructure with a previous phase transformation during reheating. Such a condition equates to the situation in the STA oxidation experiments. For the IMC-B test, a columnar grain structure appears [33]. The explained mechanism at the surface remains the same.

4.2. *Surface defect formation*

The varying results regarding surface crack formation greatly depend on the underlying cooling cycle. A change from cooling cycle 1 to cooling cycle 2 generally leads to increased cracking, which is due to the intergranular oxidation caused

by the liquid fayalite phase. These surface micro-defects form at higher temperatures, leading to stress concentration during subsequent mechanical loading. If tensile stresses are applied to steel at temperatures of low ductility, the micro-defects lead to a further drastic decrease in surface ductility. Nonetheless, Krobath et al. [4] showed that for temperatures of high ductility, the micro-defects did not affect the surface ductility. This applies for steel 2 and the temperatures 700 and 1100 °C, comparing cooling strategies 1 and 2. The same is valid for steel 1, and at 700 °C for steel 3.

As already mentioned, the Si content strongly influences the depth and ratio of forming micro-defects. When the formation of intergranular oxidation is suppressed, the susceptibility to cracking is drastically decreased, as it can be seen by comparing steel 2 after cooling cycle 1 and steel 1 after cooling cycle 2. With steel 1, the number of cracks does not increase further despite the stronger oxidation in cooling cycle 2. The total number of cracks is even slightly reduced for steel 1, and the critical strain for the samples of these two steel grades is similar, with the lowest values of about 2.5% at 850 °C. A typically known maximum mechanically induced strain value during straightening in continuous casting ranges up to ~2% [3,41].

In contrast, for steel 2, a change in the cooling cycle leads to a massive increase in detected cracks and a significant decrease in the critical strain. As a result of the complete damage to the surface austenite grains by intergranular oxidation, crack networks were formed. The results of steel 3 correspond to those of steel 2, with a total number of cracks in the range of 800 and a critical strain in the range of 2% or even lower. Therefore, it can be deduced that as soon as a corresponding intergranular oxidation is present, the quantification parameters crack number and critical strain are hardly influenced anymore, which is mainly affected by the Si content in the current work. Under the investigated test parameters for cooling cycle 2, an increased risk of cracking during the straightening process could be assumed in the temperature range of 850–950 °C for steel 2 and for steel 3 in the temperature range of 850–1100 °C. Comparing the data in Fig. 9 reveals that the ductility trough for steel 1 and steel 2 lies in the temperature range around 900 °C. For steel 3, an expansion of the ductility trough towards higher temperatures can be seen.

According to the grain size evaluation for steel 2 by Krobath et al. [43] and the values measured in this publication for steels 1 and 3, a minor influence of a difference in grain size on the surface crack formation can be disregarded. The measured surface austenite grain size for cooling cycle 2 at 900 °C is 829 μm for steel 1 and 733 μm for steel 3. Steel 2 has the smallest measured grain size of 607 μm for cooling cycle 2 and 538 μm for cooling cycle 1. All values given refer to the mean equivalent circle diameter (ECD), which is why the influence of intergranular oxidation on crack formation is considerably more significant in the current study.

5. Conclusion

In this publication, the influence of intergranular oxidation, resulting from higher silicon and oxidation at 1200 °C, on surface crack formation in a bending test at 700 °C to 1100 °C was investigated for a 0.17% C construction steel. The investigations were performed by means of the IMC-B test and simultaneous thermal analysis (STA). The steel was tested for different Si contents and cooling strategies. The following results can be highlighted:

- The formation of intergranular oxidation for cooling cycle 2 is favored by the infiltration of a liquid phase along the austenite grain boundaries. EDS analysis confirms the presence of a silicon-enriched oxide phase. This can be attributed to the low melting fayalite-wüstite eutectic. A cooling cycle with lower temperatures leads to weaker oxidation and only few intergranular oxidations due to the mostly missing low melting compound.
- Intergranular oxidation in steel 1 is due to traces. The depth of intergranular oxidation for cooling cycle 2 increases with rising Si content and is higher than 16 μm for steels 2 and 3.
- The temperature profiles of IMC-B cooling cycle 2 were successfully replicated in the STA. Repeated tests in the STA demonstrated the reproducibility of the temperature profile and the depth of the intergranular oxidation. The composition of the formed phases and internal oxides correspond to those of the IMC-B samples. In combination with the knowledge from the IMC-B test regarding surface ductility, oxidation experiments on the STA offer a time-saving tool for the prediction of intergranular oxidation and subsequently, to make a statement about their influence on surface crack formation.
- The intergranular oxidation formed during high-temperature oxidation leads to a significantly facilitated crack formation during the bending process in the IMC-B test in a temperature range where surface ductility is reduced. With increasing Si content, the number of cracks rises. The critical strain for steels 2 and 3 is significantly reduced compared to steel 1. For bending temperatures with good surface ductility, the influence of the present intergranular oxidation on surface crack formation is negligible. Furthermore, it has been clarified how surface cracking in the continuous casting process is affected due to silicon-induced intergranular oxidation.
- For steel 2 in the temperature range of 850–950 °C and for steel 3 in the temperature range of 850–1100 °C, the critical strain values for the formation of two cracks are occasionally less than two percent, which makes them crucial for the straightening process of continuous casting. The appearing cracks are located at the austenite grain boundaries and partially network-like.

Declaration of competing interest

The authors declare that they have no known competing financial interests or personal relationships that could have appeared to influence the work reported in this paper.

Acknowledgement

The authors gratefully acknowledge the funding support of K1-MET GmbH, metallurgical competence center. The research program of the K1-MET competence center is supported by COMET (Competence Center for Excellent Technologies), the Austrian program for competence centers. COMET is funded by the Federal Ministry for Climate Action, Environment, Energy, Mobility, Innovation and Technology, the Federal Ministry for Labour and Economy, the Federal States of Upper Austria, Tyrol and Styria as well as the Styrian Business Promotion Agency (SFG) and the Standortagentur Tyrol. Furthermore, Upper Austrian Research GmbH continuously supports K1-MET. Beside the public funding from COMET, this research project is partially financed by the scientific partner Montanuniversitaet Leoben and the industrial partners Primetals Technologies Austria GmbH and voestalpine Stahl GmbH.

REFERENCES

[1] Xia G, Burgstaller K, Fürst C, Harrer B, Milosch E, Samoilov A. Influence of steel composition on crack formation on the continuous casting steel slab. In: Proceeding of the 8th European continuous casting conference. Austria: Graz; 2014 June. p. 729–39. 23–26.
[2] Dippenaar RJ, Moon SC, Szekeres ES. Strand surface cracks – the role of abnormally large prior austenite grains. In: Proceeding of the association for iron & steel Technology; 2007 May 1–4. p. 833–43. Cleveland, USA.
[3] Szekeres ES. A review of strand castings factors affecting transverse cracks. In: Proceeding of the 6th international conference on clean steel; 2002 June 10–12. p. 324–38. Balatonfüred, Hungary.
[4] Krobath R, Bernhard C, Ilie S, Six J, Hahn S, Pennerstorfer P. The role of grain boundary oxidation on surface crack formation under continuous casting conditions. Berg Huettenmaenn Monatsh 2019;164(11):461–5.
[5] Melford DA. The influence of residual and trace elements on hot shortness and high temperature embrittlement. Phil Trans Roy Soc Lond 1980;295(1413):89–103.
[6] Wolf MM. Fine intergranular surface cracks in bloom casting. ISIJ Int 1984;24(5):351–8.
[7] Chen RY, Yuen WYD. Isothermal and step isothermal oxidation of copper-containing steels in air at 980–1220°C. Oxid Met 2005;63(3–4):145–68.
[8] Imai N, Komatsubara N, Kunishige K. Effects of Cu and other tramp elements on steel properties. Effect of Cu and Ni on hot workability of hot-rolled mild steel. ISIJ Int 1997;37(3):224–31.
[9] Kunishige K, Hatano M. Surface hot-shortness of steels induced by a small amount of copper and tin from scrap steels and its suppression methods. Mater Sci Forum 2007;539–543:4113–8.
[10] Sampson E, Sridhar S. Effect of water vapor during secondary cooling on hot shortness in Fe-Cu-Ni-Sn-Si alloys. Metall Mater Trans B 2014;45(5):1769–81.
[11] Seo SJ, Asakura K, Shibata K. Effects of Cu and other tramp elements on steel properties. Effects of 0.4% Si and 0.02% P additions on surface hot shortness in 0.1%C-0.5%Mn steels containing 0.5% Cu. ISIJ Int 1997;37(3):240–9.
[12] Shibata K, Seo S-J, Kaga M, Uchino H, Sasanuma A, Asakura K, et al. Suppression of surface hot shortness due to Cu in recycled steels. Mater Trans 2002;43(3):292–300.
[13] Webler BA, Sridhar S. Evolution and distribution of the copper-rich phase during oxidation of an iron–0.3wt% Copper alloy at 1150°C. ISIJ Int 2008;48(10):1345–53.
[14] Yeşiltepe S, Şeşen MK. High-temperature oxidation kinetics of Cu bearing carbon steel. SN Appl Sci 2020;2(4).
[15] Yin L, Sridhar S. Effects of small additions of tin on high-temperature oxidation of Fe-Cu-Sn alloys for surface hot shortness. Metall Mater Trans B 2010;41(5):1095–107.
[16] Chen RY, Yuen WYD. Copper enrichment behaviours of copper-containing steels in simulated thin-slab casting processes. ISIJ Int 2005;45(6):807–16.
[17] Yin L, Sampson E, Nakano J, Sridhar S. The effects of nickel/tin ratio on Cu induced surface hot shortness in Fe. Oxid Met 2011;76(5–6):367–83.
[18] Cruz RA, Romero SA, Vargas RM, Hallen LM. Thermodynamic analysis of the SiO2–NiO–FeO system. J Non-Cryst Solids 2005;351(16–17):1359–65.
[19] Suarez L, Schneider J, Houbaert Y. High-temperature oxidation of Fe- Si alloys in the temperature range 900-1250°C. DDF 2008;273–276:661–6.
[20] Liu X, Cao G, He Y, Jia T, Liu Z. Effect of temperature on scale morphology of Fe-1.5Si alloy. J Iron Steel Res Int 2013;20(11):73–8.
[21] Fukagawa T, Okada H, Maehara Y. Mechanism of red scale defect formation in Si-added hot-rolled steel sheets. ISIJ Int 1994;34(11):906–11.
[22] Melfo W, Bolt H, Rijnders M, Staalman D, Castro CB, Crowther D, et al. Experimental study on primary scale formation and descalability on steels containing Ni and Ni+Si. ISIJ Int 2013;53(5):866–73.
[23] Yuan Q, Xu G, Liang W, Zhou M, Hu H. Effects of oxygen concentration on the passivation of Si-containing steel during high-temperature oxidation. Corrosion Rev 2018;36(4):385–93.
[24] Taniguchi S, Yamamoto K, Megumi D, Shibata T. Characteristics of scale/substrate interface area of Si-containing low-carbon steels at high temperatures. Mater Sci Eng, A 2001;308(1–2):250–7.
[25] Kizu T, Yasunobu N, Toru I, Yoshihiro H. Intergranular and internal oxidation during hot-rolling process in ultra-low carbon steel. ISIJ Int 2002;42(2):206–14.
[26] Fukagawa T, Okada H, Maehara Y, Fujikawa H. Effect of small amount of Ni on hydranlic-descaling-ability in Si-added hot-rolled steel sheets. Tetsu-To-Hagane 1996;82(1):63–8.
[27] Okada H, Fukagawa T, Ishihara H, Okamoto A, Azuma M, Matsuda Y. Prevention of red scale formation during hot rolling of steels. ISIJ Int 1995;35(7):886–91.
[28] Zeze M, Tanaka A, Tsujino R. Formation mechanism of sliver-type surface defect with oxide scale on sheet and coil. Tetsu-To-Hagane 2001;87(2):85–92.
[29] Bernhard C, Linzer B, Presoly P, Watzinger I, Watzinger J. Evaluation of AHSS concepts with a focus on the product properties and appropriate casting characteristics of Arvedi ESP thin slab casters. In: Proceeding of the 5th international conference on advances in solidification processes. Austria: Salzburg; 2019 June. p. 17–21.
[30] Ohba Y, Yamashita Y, Ohno K, Maeda T, Nishioka K, Shimizu M. Formation mechanism of oxide particles in

subscale layer around surface cracks of steel. Tetsu-To-Hagane 2009;95(7):531–40.
[31] Auinger M, Praig VG, Linder B, Danninger H. Grain boundary oxidation in iron-based alloys, investigated by 18O enriched water vapour – the effect of mixed oxides in binary and ternary Fe–{Al, Cr, Mn, Si} systems. Corrosion Sci 2015;96:133–43.
[32] Lee DB, Choi JW. High temperature oxidation of steels in air and CO2–O2 atmosphere. Oxid Met 2005;64(5–6):319–29.
[33] Krobath R, Bernhard C. Experimental quantification of critical parameters for prediction of surface crack formation in continuous casting. steel research int 2020;20:2000234.
[34] Preßlinger H, Mayr M, Tragl E, Bernhard C. Assessment of the primary structure of slabs and the influence on hot- and cold-rolled strip structure. steel research int 2006;77(2):107–15.
[35] Reiter J, Bernhard C, Presslinger H. Austenite grain size in the continuous casting process: metallographic methods and evaluation. Mater Char 2008;59(6):737–46.
[36] Zhang X, Zhu H, Huang W, Shi B, Tieu AK. Investigation on slab continuous straightening technology and deformation analysis. Int J Mater Prod Technol 2013;47:126–37.
[37] Krobath M, Krobath R, Bernhard C, Ecker W. Elasto-viscoplastic material model of a directly-cast low-carbon steel at high temperatures. Materials 2020;13(10).
[38] Krajewski P, Krobath R, Bernhard C, Miettinen J, Louhenkilpi S, Ilie S, et al. A novel approach for the simulation of surface crack formation in continuous casting. Berg Huettenmaenn Monatsh 2015;160(3):109–16.
[39] Gaiser G, Presoly P, Bernhard C. High-temperature oxidation of steel under linear flow rates of air and water vapor—an experimental determined set of data. Metals 2023;13(5):892.
[40] Zhou M, Xu G, Hu H, Yuan Q, Tian J. The morphologies of different types of Fe_2SiO_4–FeO in Si-containing steel. Metals 2017;7(1):8.
[41] Mintz B, Crowther DN. Hot ductility of steels and its relationship to the problem of transverse cracking in continuous casting. Int Mater Rev 2010;55(3):168–96.
[42] Crowther DN. The effects of microalloying elements on cracking during continuous casting. In: The use of vanadium in steel - proceedings of the vanitec symposium; 2001 Oct. p. 99–131. Beijing, China.
[43] Krobath R, Bernhard C, Ilie S, Six J, Hahn S, Pennerstorfer P. The role of grain boundary oxidation on surface crack formation under continuous casting conditions. In: Proceeding of the 4th European steel Technology and application days. Germany: Duesseldorf; 2019 June. p. 24–8.